

Compression of 3D Ultrasound Data Using Wavelet Bases on Intervals

Otmar Scherzer¹, Armin Schoisswohl^{1*} and Alfred Kratochwil²

¹ Industrial Mathematics Institute, Johannes Kepler University, Linz, Austria

² University Clinic for Radiotherapy and Radiobiology, AKH-Vienna, Austria

April 12, 2019

Abstract

One purpose of telemedicine is the transfer of medical data via networks for diagnostic purposes. The large size of 3D medical image data makes it almost impossible to submit it uncompressed via relatively slow networks, like e.g. the Internet. In this paper we describe some wavelet based algorithms for the compression of medical 3D ultrasound data. Using compression algorithms based on orthogonal or biorthogonal wavelets as well as the standardized compression algorithm MPEG II results in artifacts of the compressed image especially near the boundary. To prevent such distortions wavelet bases on intervals are used in this paper. We apply compression algorithms with standard wavelet bases and wavelets on the interval as well as MPEG II compression to clinical 3D ultrasound data and evaluate the compressed data from a medical point of view.

Keywords: wavelets on intervals, data compression, 3D ultrasound, medical diagnostics, telemedicine

1 Introduction

Medical 3D ultrasound data sets are 3-dimensional tensors of 8 bit grayscale values with typical sizes between 128^3 and 256^3 voxels. Such large amounts of data (approximately 2 – 16 Megabytes) can hardly be transferred in reasonable times for telediagnostic purposes via slow networks.

Lossy compression algorithms aim to reduce the amount of data and simultaneously preserve the essential information in the data set. There are a number of standardized compression algorithms, like JPEG (see e.g. Pennebaker and Mitchell (1993)), which is based on discrete cosine transform, for 2D images and MPEG (see e.g. Le Gall (1991)) for image sequences. In the recent years

*Industrial Mathematics Institute, Johannes Kepler University, A-4040 Linz, Altenberger Straße 69, Austria (email: schoisswohl@indmath.uni-linz.ac.at)

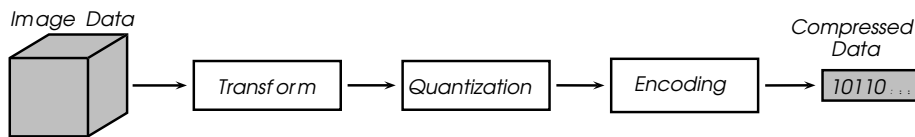


Figure 1: Schematic representation of the wavelet compression algorithm

wavelet based compression algorithms have gained increasing importance since they can be adopted flexible to the data to be compressed (see e.g. Antonini *et al.* (1992); DeVore *et al.* (1992); Maass *et al.* (1997)). Wavelet compression has proved to be an efficient method for the compression of higher dimensional medical image data, like e.g. 3D X-ray data Benoit-Cattin *et al.* (1997), or CT and MR data Wang and Huang (1996).

To our knowledge wavelet based compression algorithms for 3D data sets in clinical applications have just been implemented using 3-dimensional products of orthonormal and biorthonormal compactly supported wavelet bases on the real line. Formally this approach requires to extend the data set onto \mathbb{R}^3 . Usually symmetric or periodic extension along the axes is used. All artificial extensions produce more or less significant artifacts near the boundary. By using tensor products of orthonormal wavelet bases on intervals such artifacts can be avoided.

The outline of this paper is as follows: In Section 2 we outline compression algorithms using tensor products of orthonormal bases of compactly supported wavelets Daubechies (1988, 1993) and wavelets on the interval Cohen *et al.* (1993); Chyzak *et al.* (1999). In Section 3 we compare numerical results obtained with wavelets on the interval and wavelets on the real line as well as MPEG II compressed data and present a subjective evaluation from a medical point of view.

2 Wavelet-Based Lossy Data Compression

A lossy data compression algorithm consists of three successive steps (cf. Figure 1): *transformation* to represent the data in a compact form, *quantization* to eliminate “non essential” information and finally *entropy coding* for efficient storage of the quantized data.

For the reconstruction from the compressed representation it is necessary to reverse these three steps. Transformation and entropy coding are invertible while quantization eliminates information and is therefore not invertible.

In the following we outline the three steps of a wavelet compression algorithm with particular emphasize on application to 3D ultrasound data.

2.1 Wavelet Transform

Wavelets are a family of one-dimensional basis functions $\psi_{m,k}$. Each function $\psi_{m,k}$ is obtained from a single *mother wavelet* ψ by translation and dilation, i.e.

$$\psi_{m,k}(x) := 2^{-m/2}\psi(2^{-m}x - k).$$

The mother wavelet ψ is related via the so called *refinement equation* to the *scaling function* ϕ in the following way

$$\psi(x) := \sqrt{2} \sum_{k \in \mathbb{Z}} (-1)^k h_{1-k} \phi(2x - k),$$

where the function ϕ is itself the solution of the *dilation equation*

$$\phi(x) = \sqrt{2} \sum_{k \in \mathbb{Z}} h_k \phi(2x - k).$$

Both the scaling function and the wavelet are completely determined by the sequence of filter coefficients $\{h_k\}$. The construction of filter sequences such that the resulting wavelets have compact support and form an orthonormal Riesz basis has been introduced by Daubechies Daubechies (1992, 1988, 1993).

Orthonormal compactly supported wavelets are bases for functions on the real line \mathbb{R} . Thus they are not particularly suited for the expansion of functions which are defined on compact intervals $D \subset \mathbb{R}$. Recently the construction of orthogonal wavelet bases on compact intervals has been established Cohen *et al.* (1993); Chyzak *et al.* (1999).

The main difference to wavelets on \mathbb{R} is that no longer the wavelets $\psi_{m,k}$ can be obtained by translating and dilating a single mother wavelet ψ . But still it is possible to gain refinement equations, which are most essential for the implementation of an efficient transform algorithm. It can be shown that for orthonormal wavelets Cohen *et al.* (1993); Chyzak *et al.* (1999) there exist refinement matrices H and G such that the scaling functions $\phi_{m,k}$ and wavelets $\psi_{m,k}$ satisfy

$$\begin{aligned} \phi_{m+1,k} &= \sqrt{2} \sum_{l \in Z_m} H_{k,l} \phi_{m,l}, \\ \psi_{m+1,k} &= \sqrt{2} \sum_{l \in Z_m} G_{k,l} \phi_{m,l}, \end{aligned}$$

where Z_m is a finite set of integers depending on the interval and the scale m . Let

$$V_m := \overline{\text{span} \{ \phi_{m,k}, k \in Z_m \}},$$

and

$$W_m := \overline{\text{span} \{ \psi_{m,k}, k \in Z_m \}}.$$

Then the sequence of *scaling spaces* V_m forms a multiresolution analysis on $L^2(D)$. The *wavelet space* W_m is defined as the orthogonal complement of V_m in V_{m-1} . Consequently the space of square integrable functions on D can be represented as the orthogonal direct sum

$$L^2(D) = \overline{\bigoplus_{m \in \mathbb{Z}} W_m}.$$

As a consequence each function $f \in L^2(D)$ can be decomposed into its wavelet expansion

$$f = \sum_{m,k} d_{m,k} \psi_{m,k},$$

where the wavelet coefficients $d_{m,k}$ are given by

$$d_{m,k} = \langle f, \psi_{m,k} \rangle := \int_D f(x) \psi_{m,k}(x) dx.$$

A difficulty associated with the numerical calculation of $d_{m,k}$ is due to the fact that there is no analytical representation of the wavelets and scaling functions. However, if the projection $P_m f$ of f onto the space V_m is known, i.e.

$$P_m f = \sum_{k \in Z_m} f_{m,k} \phi_{m,k},$$

then the coefficients $f_{m+1,k}$ and $d_{m+1,k}$ of the projections

$$\begin{aligned} P_{m+1} f &= \sum_{k \in Z_{m+1}} f_{m+1,k} \phi_{m+1,k}, \\ Q_{m+1} f &= \sum_{k \in Z_{m+1}} d_{m+1,k} \psi_{m+1,k}, \end{aligned}$$

onto the coarser spaces V_{m+1} and W_{m+1} , respectively, can be computed using the *Mallat transform*

$$\begin{aligned} f_{m+1,k} &= \sum_{l \in Z_m} H_{k,l} f_{m,l}, \\ d_{m+1,k} &= \sum_{l \in Z_m} G_{k,l} f_{m,l}, \end{aligned}$$

for all $k \in Z_{m+1}$. Its inversion is given by

$$f_{m,k} = \sum_{l \in Z_{m+1}} H_{l,k} f_{m+1,l} + \sum_{l \in Z_{m+1}} G_{l,k} d_{m+1,l},$$

for all $k \in Z_m$. Note that this formulation of the Mallat transform also holds for wavelets on the real line Mallat (1989) by setting $H_{k,l} := h_{l-2k}$, $G_{k,l} := (-1)^k h_{1-k}$ and $Z_m := \mathbb{Z}$.

2.1.1 n -dimensional Product Wavelets

A generalization of wavelets to higher dimensions is implemented by a tensor product ansatz. We define the n -dimensional product wavelet $\Psi_{m,k}^\iota$ by

$$\Psi_{m,k}^\iota(x) := \psi_{m,k_1}^{\iota_1}(x_1) \cdots \psi_{m,k_n}^{\iota_n}(x_n),$$

where $x = (x_1, \dots, x_n)$, $k = (k_1, \dots, k_n) \in Z_m$, $m \in \mathbb{Z}$, and $\iota = (\iota_1, \dots, \iota_n) \in I := \{0, 1\}^n$. The functions $\psi_{m,k_i}^0 := \phi_{m,k_i}$ and $\psi_{m,k_i}^1 := \psi_{m,k_i}$ denote the 1-dimensional scaling function and wavelet, respectively. In this setting $\Psi_{m,k}^0$ denote the n -dimensional scaling functions.

Similar to the 1-dimensional setting every on a n -dimensional parallelepiped $D \subset \mathbb{R}^n$ square integrable function $f \in L^2(D)$ can be represented by its wavelet series expansion

$$f = \sum_{m \in \mathbb{Z}} \sum_{k \in Z_m} \sum_{\iota \in I^*} d_{m,k}^\iota \Psi_{m,k}^\iota,$$

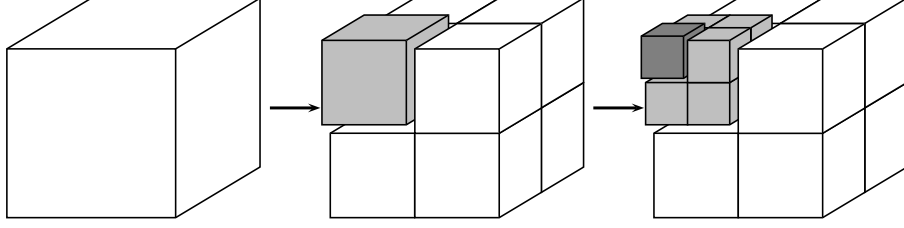


Figure 2: Successive decomposition of the 3D data set into subbands by the 3D Mallat transform algorithm.

where $I^* := I \setminus \{0\}$ and

$$d_{m,k}^\iota := \langle f, \Psi_{m,k}^\iota \rangle = \int_D f(x) \Psi_{m,k}^\iota(x) dx.$$

The n -dimensional Mallat transform allows to calculate the wavelet coefficients $d_{m+1,k}^\iota$, representing the function f at scale $m+1$, from the coefficients $d_{m,k}^0$ representing f at scale m ($P_m f = \sum d_{m,k}^0 \Psi_{m,k}^0$):

$$d_{m+1,k}^\iota = \sum_{l \in Z_m} H_{k_n, l_n}^{\iota_n} \cdots H_{k_1, l_1}^{\iota_1} d_{m,l}^0, \quad (1)$$

where $H_{k,l}^0 := H_{k,l}$ and $H_{k,l}^1 := G_{k,l}$. The inverse n -dimensional Mallat transform is given by

$$d_{m,k}^0 = \sum_{\iota \in I} \sum_{l \in Z_{m+1}} H_{l_n, k_n}^{\iota_n} \cdots H_{l_1, k_1}^{\iota_1} d_{m+1,l}^\iota. \quad (2)$$

2.1.2 Application to Compression of 3D Ultrasound Data

We represent the 3D ultrasound data set f by

$$f := \sum_{k \in Z_0} d_{0,k}^0 \Psi_{0,k}^0,$$

where $d_{0,k}^0$ is the gray value of the data set at position $k \in Z_0 \subset \mathbb{Z}^3$. Application of the Mallat transform decomposes the coefficients $d_{m,k}^0$ into eight subbands $S_{m+1}^\iota := \{d_{m+1,k}^\iota, k \in Z_{m+1}\}$, $\iota \in \{0,1\}^3$ with $|S_m^\iota| = 8|S_{m+1}^\iota|$. Successive application of the Mallat transform (1) yields that for $M \in \mathbb{N}$ (cf. Figure 2)

$$f = \sum_{k \in Z_M} d_{M,k}^0 \Psi_{M,k}^0 + \sum_{m=1}^M \sum_{\iota \in I^*} \sum_{k \in Z_m} d_{m,k}^\iota \Psi_{m,k}^\iota. \quad (3)$$

The inverse Mallat transform (2) allows to reconstruct the data $d_{0,k}^0$ from the coefficients $d_{M,k}^0$ and $d_{m,k}^\iota$, $\iota \in I^*$, $m = 1, \dots, M$. Any wavelet based compression algorithm utilizes the representation (3) and further processes the coefficients $d_{M,k}^0$ and $d_{m,k}^\iota$.

2.2 Equidistant Scalar Quantization

The 3D Mallat transform produces non-integer wavelet coefficients $d_{m,k}^t$, even if the provided input data $d_{0,k}^0$ consists of integer gray values. To store the real wavelet coefficients efficiently they are clustered by identifying the values in a cluster by an integer value.

For clustering we use equidistant scalar quantization, where each coefficient $d_{m,k}^t$ is scaled and rounded to the nearest integer value, i.e.

$$d_{m,k}^t \mapsto \varrho(d_{m,k}^t / q_m^t),$$

where ϱ denotes the rounding operator. An increasing quantization parameter increases the loss of information and a higher compression rate can be achieved. Thus the quantization parameters q_m^t provide a compromise between quality of the reconstruction and compression rate.

Determination of the quantization parameters q_m^t to achieve a given compression rate leads to the constrained minimization problem of bit allocation (see e.g. Bradley *et al.* (1993); Strang and Nguyen (1996)).

2.3 Entropy Coding

The quantized data can be stored efficiently using entropy coding. We use baseline coding, a combination of runlength coding and Huffman coding as it is also used in JPEG. For a detailed description of these algorithms we refer to Pennebaker and Mitchell (1993) or Strang and Nguyen (1996).

3 Numerical Results

In this section we discuss the medical diagnostics of 3D ultrasound data sets which are reconstructed from compressed data. We consider the following algorithms:

WBI: Wavelet compression using 3D tensor products of *Daubechies 4* wavelets on the interval Cohen *et al.* (1993).

WBR: Wavelet compression using 3D tensor products of *Daubechies 4* wavelets on \mathbb{R} Daubechies (1993). For the wavelet expansion of the data in terms of wavelets one needs samples of the 3D ultrasound data on the whole set \mathbb{Z}^3 . Therefore the finite data set is extended periodically over its boundaries.

MPEG: Compression with the video encoding standard MPEG II. Here the data set is split into a series of transversal slices which are encoded as a movie sequence by the MPEG encoder.

The medical 3D ultrasound data sets considered in these examples were acquired with a Kretztechnik Voluson 530D diagnostic ultrasound system. The numerical experiments were performed on a Digital Alpha workstation with a 433 MHz 21164 CPU under Digital Unix. With this equipment the wavelet compression of a 3D ultrasound data set of approximately 10^7 voxels requires approximately 3.1 CPU seconds.

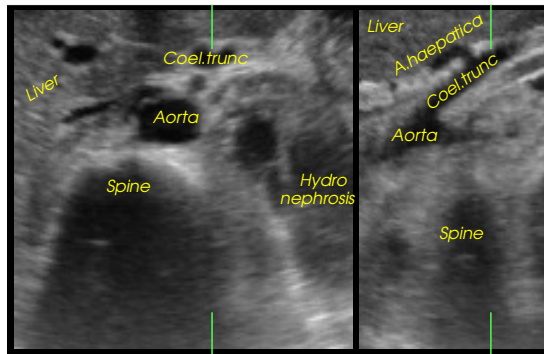


Figure 3: Transversal (left) and sagittal slice (right) of a 3D ultrasound data set of the upper abdomen

3.1 Upper abdomen

In a first example we consider a 3D ultrasound data set which shows a part of the upper abdomen. Figure 3 displays a transversal and a sagittal slice of this data set. The images show the Aorta near the branching of the Coeliac Trunc, part of the liver with vessel structures and the Arteria Haepatica, and, on the backside, the spine and part of a kidney with a Hydro Nephrosis.

The corresponding slices of the reconstruction from 40 : 1 compressed data are shown in Figure 4. A comparison with the slices in Figure 3 reveals that essential diagnostic information, such as small vessel structures and vascular walls, are preserved qualitatively correct in the WBI and WBR compressed data sets (top and middle). These data sets show a subjective similar quality although the peak-signal-to-noise-ratio (PSNR) of the WBI compressed data is 33.28 dB and therefore 1 dB higher than the PSNR of the WBR compressed data (32.28 dB). The blurring of the tissue introduced by the compression is perceptible but does not affect the clinical diagnosis. The transversal slice of the MPEG compressed data shows typical 8×8 blocking artifacts resulting from the block-based discrete cosine transform used in MPEG. These blocking artifacts are also perceptible in the sagittal slices as horizontal edges. The vertical edges in the sagittal slices result from the per-slice encoding of the MPEG encoder. Due to these artifacts essential diagnostic content, especially fine structures as vascular walls, is lost in a 40 : 1 MPEG compressed data set. This fact is also reflected by a significant lower PSNR of 30.39 dB.

Figure 5 shows zooms of three successive transversal slices of the original data (middle) as well as slices of the reconstructions from the WBI (left) and MPEG compressed (right) data sets. It is clearly perceptible that the quality of the MPEG compressed data varies much from slice to slice which is due to the coding mechanism for time frames used in MPEG.

3.2 Human fetus

In a second example we consider the 3D ultrasound data set of the head of a 30 week old human fetus shown in Figure 6. A plot of the PSNR of the

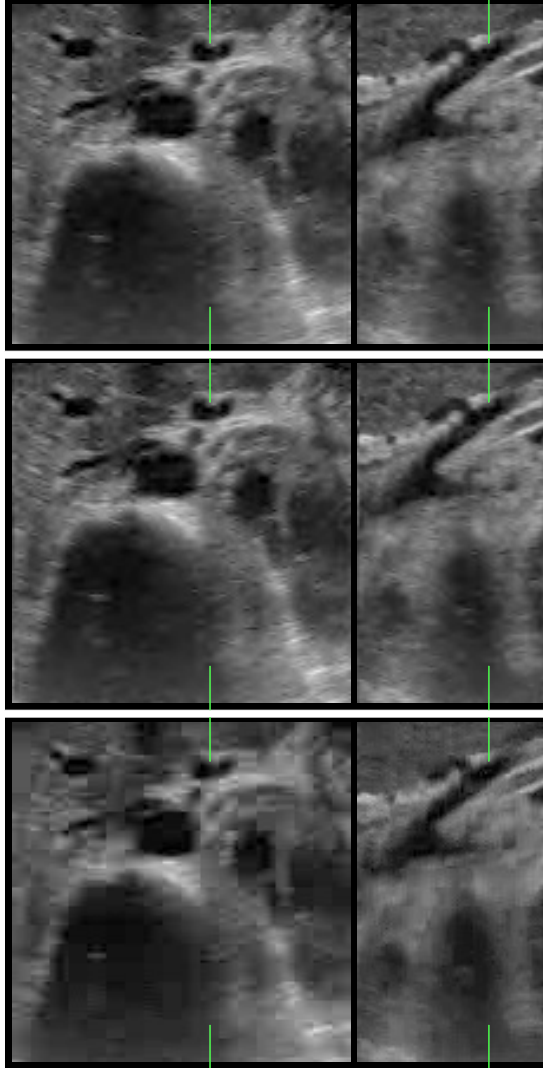


Figure 4: Transversal (left) and sagittal slice of a 3D ultrasound data set of the upper abdomen: reconstructions from a 40 : 1 compression using WBI (top), WBR (middle) and MPEG (bottom)

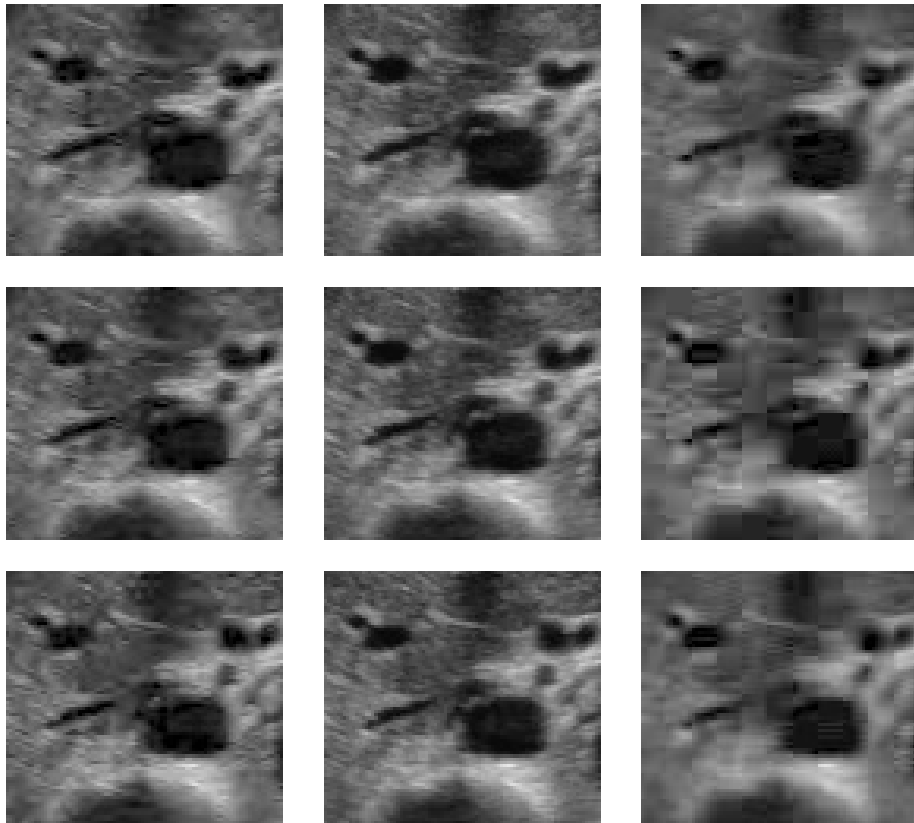


Figure 5: Zooms of three consecutive transversal slices out of the wavelet compressed (left), original (middle) and the MPEG (right) compressed data set.

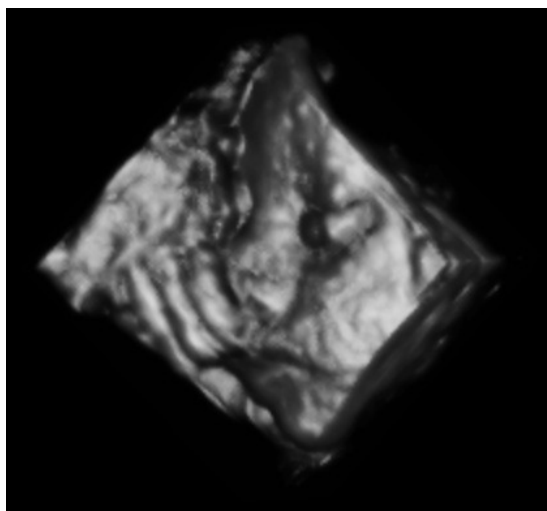


Figure 6: Rendered visualization of a 3D ultrasound data set of a 30 week old human fetus

reconstruction over the compression rate (Figure 7) shows that WBI performs significantly better than WBR, especially at higher compression rates.

At a compression rate of 44 : 1 the PSNR of the WBI compressed data is 31.99 dB and approximately 0.9 dB higher than the PSNR of the WBR compressed data (31.07 dB). However if one considers the PSNR of the transversal 2D slices (Figure 8) then it is visible that WBI compression performs significantly better than WBR compression near the boundaries of the data set (Slices No. 0 – 5 and 123 – 128). This performance loss of WBR is an effect of discontinuities that are introduced by periodic extension of the data set. These jumps cannot be recovered without major artifacts. This effect is also clearly visible in 2D slices of the 3D data set (Figure 9).

Acknowledgements

The work of O.S. and A.S. was supported by the Austrian “Forschungsförderungsfonds für die gewerbliche Wirtschaft” (FFF), Grant 200354. The authors thank the company Kretztechnik AG, Zipf, Austria, for the allowance to publish this work.

References

- Antonini, M., Barlaud, M., Mathieu, P., and Daubechies, I. (1992). Image coding using wavelet transform. *IEEE Trans. Image Proc.*, 1(2), 205–220.
- Benoit-Cattin, H., Baskurt, A., Turjman, F., and Prost, R. (1997). 3D medical image coding using separable 3D wavelet decomposition and lattice vector quantization. *Signal Process.*, 59(2), 139–153.

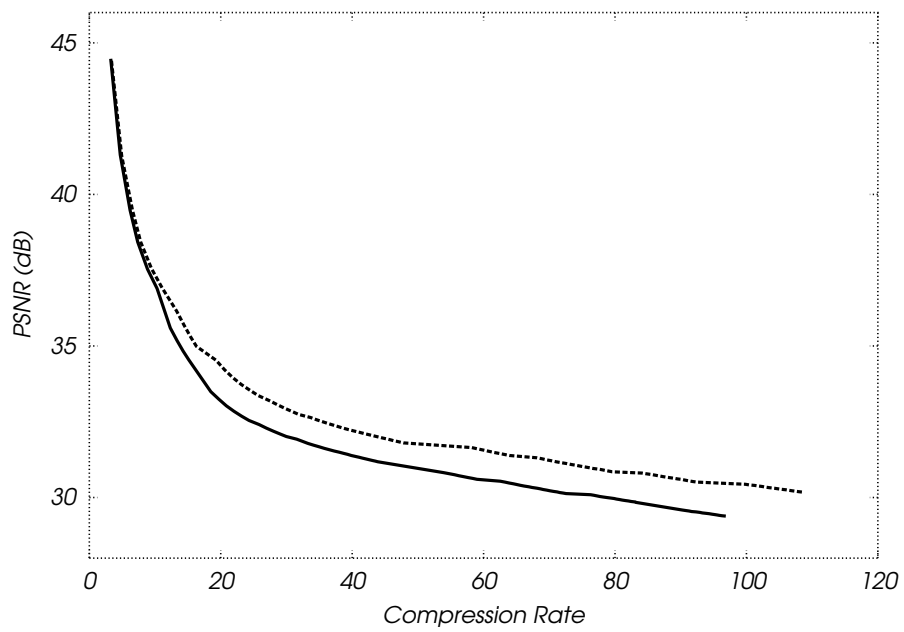


Figure 7: PSNR of the reconstructed 3D ultrasound data set at different compression rates: WBI (dashed) is superior to WBR especially at higher compression rates

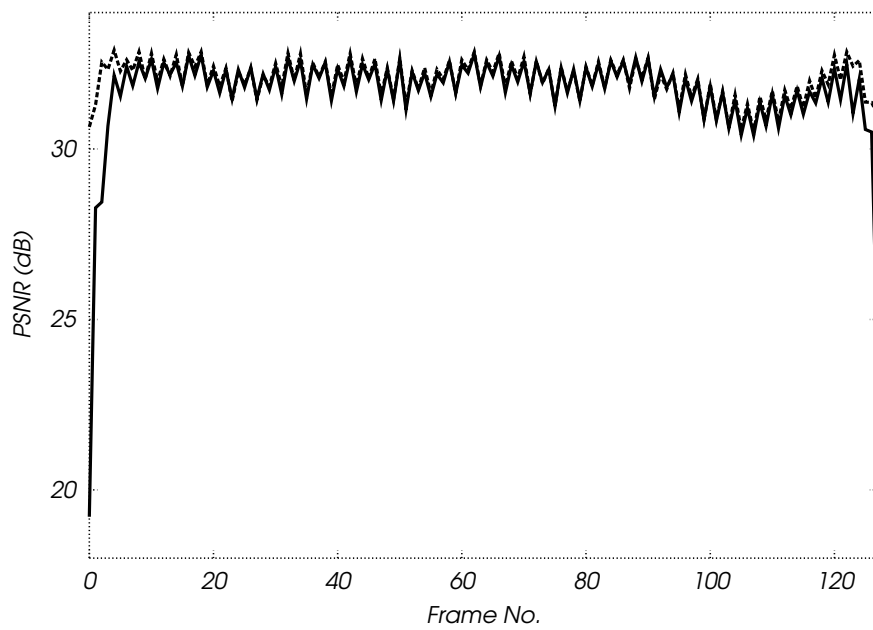


Figure 8: PSNR of transversal slices of reconstructions from 44 : 1 compressed data: WBI (dashed) is significantly superior to WBR (solid) near the boundaries of the 3D data set

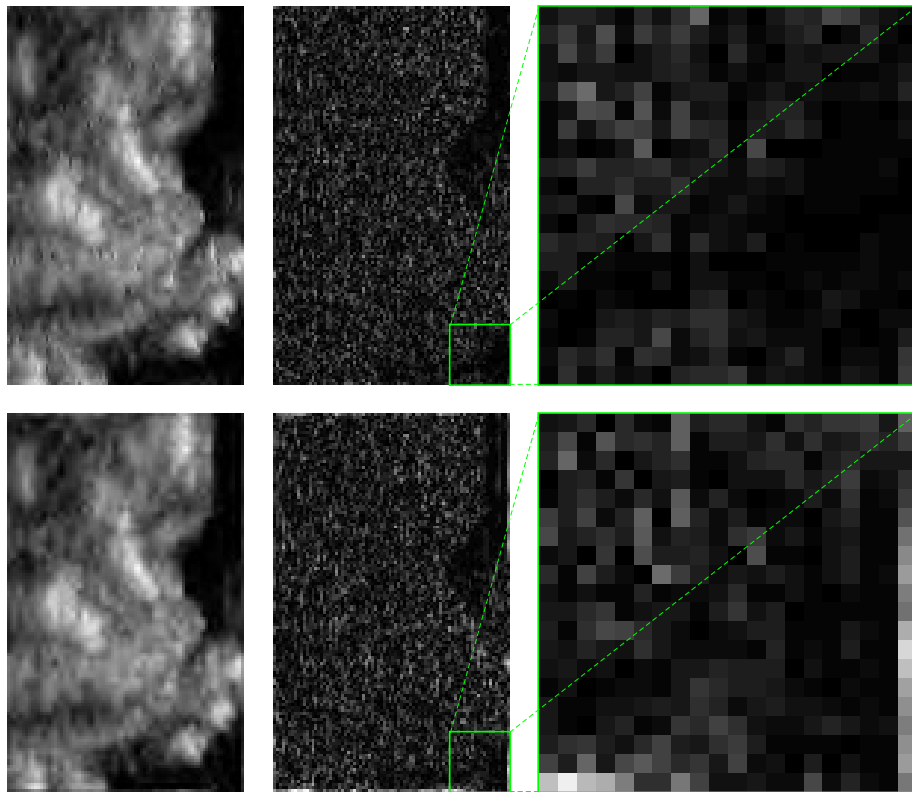


Figure 9: Saggital slice of reconstructions from 44 : 1 compressed 3D ultrasound data: WBI (top) and WBR (bottom), reconstruction (left), difference (middle) and zoom of the difference (right). The boudary artifacts in the WBR reconstruction are clearly visible

- Bradley, J.N., Brislawn, C.M., and Hopper, T. (1993). The FBI wavelet/scalar quantisation standard for gray-scale fingerprint image compression. Technical report, Los Alamos National Laboratory.
- Chyzak, F., Paule, P., Scherzer, O., Schoisswohl, A., and Zimmermann, B. (1999). Construction of orthonormal wavelets using symbolic methods and a matrix analytical approach to the construction of wavelets on the interval. *Submitted for publication*.
- Cohen, A., Daubechies, I., and Vial, P. (1993). Wavelets on the interval and fast wavelet transforms. *Appl. Comput. Harmon. Anal.*, 1(1), 54–81.
- Daubechies, I. (1988). Orthonormal bases of compactly supported wavelets. *Commun. Pure Appl. Math.*, 41(7), 901–996.
- Daubechies, I. (1992). *Ten Lectures on Wavelets*, Vol. 61 of *CBMS-NSF Regional Conference Series in Applied Mathematics*. SIAM, Philadelphia.
- Daubechies, I. (1993). Orthonormal bases of compactly supported wavelets. II: Variations on a theme. *SIAM J. Math. Anal.*, 24(2), 499–519.
- DeVore, R.A., Jawerth, B., and Lucier, B.J. (1992). Image compression through wavelet transform coding. *IEEE Trans. Inf. Theory*, 38(2/II), 719–746.
- Le Gall, D. (1991). MPEG: a video compression standard for multimedia applications. *Communications of the ACM*, 34(4), 46–58.
- Maass, P., Boskamp, T., Dicken, V., Bischoff, R., Peters, H., and Stark, H.G. (1997). *Mathematik: Schlüsseltechnologie für die Zukunft. Verbundprojekte zwischen Universität und Industrie.*, chapter Bilddatenkompression mit Wavelet-Methoden. (Image data compression using wavelet methods), pp. 385–394. Springer, Berlin.
- Mallat, S.G. (1989). A theory for multiresolution signal decomposition: The wavelet representation. *IEEE Trans. Pattern Anal. Mach. Intell.*, 11(7), 674–693.
- Pennebaker, W.B. and Mitchell, J.L. (1993). *JPEG - Still Image Data Compression Standard*. Van Nostrand Reinhold, New York.
- Strang, G. and Nguyen, T. (1996). *Wavelets and Filter Banks*. Wellesley-Cambridge Press, Wellesley, MA, USA.
- Wang, J. and Huang, H.K. (1996). Medical image compression by using three-dimensional wavelet transformation. *IEEE Trans. Medical Imaging*, 15(4), 547–554.